J. COMBIN. MATH. COMBIN. COMPUT. 127b (2025) 7245--7255

Journal of Combinatorial Mathematics and Combinatorial Computing
www.combinatorialpress.com/jcmcc

Combinatorial Press

Vibration Characteristics of Power-Split Transmission System with coupling misalignment

Zhao Ji[1,✉], Meixi Du[2], Xia Li[1]

[1] *SEW Industrial GEAR (Tianjin) Co., Ltd., Tianjin, 300457, China*

[2] *Tianjin Port NO.4 Stevedoring Co., Ltd., Tianjin, 300456, China*

ABSTRACT

In this paper, the vibration characteristics of the helical cylindrical gear split-torque transmission system with diaphragm coupling misalignment are studied. Firstly, the 14-DOF nonlinear simulation model of the helical cylindrical gear split-torque transmission system are established. To improve the model accuracy, time-varying mesh stiffness, random backlash, mesh error and bending deformation of shaft are considered respectively. Secondly, according to the nonlinear simulation model, the differential equations are established, and the differential equations are sovled with the time-varying stiffness of diaphragm coupling misalignment. Finally, the relationship between the phase of bolt group in diaphragm coupling and the asymmetric property of the split-torque transmission system is determined by numerical methods. The results show that the asymmetric property of split-torque transmission system could be effectively improved by changing the phase of bolt group in diaphragm coupling. The method is proven effectiveness by a modification work involved in this paper, and have reference significance for solving engineering problems.

Keywords: Split-torque transmission system, vibration model, diaphragm coupling, misalignment, phase difference, asymmetric property

1. Introduction

In aerospace, energy power, petrochemical, transportation and other fields, rotating machinery and equipment has been widely used. Large-scale rotating machinery and equipment are often coupled together by multiple rotors to improve the equipment's work capacity and efficiency, and the multi-rotor system requires coupling connection between the rotors, and the failure problems arising from the operation process are more complex than single rotor [1-3]. Rotor misalignment caused by rotor support height deviation from the design height is a fairly common type of failure in multi-rotor systems [4]. The so-called rotor misalignment usually means that two adjacent rotors, which should

✉ Corresponding author.
E-mail address: jidaalang@163.com (Z. Ji).
Received 15 January 2024; Revised 20 February 2024; Accepted 30 November 2024; Published Online 16 April 2025.
DOI: 10.61091/jcmcc127b-395

be coaxial by design, have different axial lines in actual operation [5]. The coupling misalignment will cause unstable movement of the rotor system, which in turn causes equipment vibration, bearing wear, shaft deflection deformation, rotor and stator friction and a series of problems, which may affect the normal operation of the equipment, and in the worst case, it will cause damage to the equipment and lead to more serious accidents, which accounts for the majority of vibration failures in rotating machinery [6-9].

Due to the existence of different types of couplings, the vibration mechanism of rotor misalignment failure is not the same [10]. Flexible couplings have special structures such as elastic elements, which can compensate for certain radial, angular, and axial displacement deviations when coupling misaligned rotors, but their own tensile angular misalignment also generates a generalized excitation force during rotation, which has an effect on the vibration characteristics of the shaft system [11-14]. Rigid coupling consists of two halves of the backrest wheel bolted together, the coupling does not have the function of compensating displacement when the rotor is not centered, but generally does not produce its own tensor angle or misalignment, but will pull the adjacent rotor into a smooth curve of the whole shaft, so that the deflection curve of the shaft system, the distribution of the internal force has changed, bearing loads, stiffness is redistributed, and thus have an impact on the vibration characteristics of the shaft system [15-19]. When the alignment deviation occurs between rotors, the bearing stiffness near the coupling is changed, the vibration transmission characteristics between rotors may change, and the vibration coupling phenomenon may occur between adjacent rotors, which causes difficulties in judging the source of vibration faults [20-22]. Therefore, the study of coupling misalignment rotor dynamics, mastering the misalignment rotor system vibration behavior analysis theory and method, not only has important theoretical significance, but also has very important practical application value [23-25].

The helical gear shunt drive system studied in this paper has an average load factor of less than 1.05 without considering external excitation, but the actual bias load situation still exists. Parallel car level (the second level of engagement) two branches of the wear comparison shown in Figure 1: parallel car level two pairs of engagement and the corresponding bearings are more serious bias load (i.e., one side of the wear is serious and the other side is almost no wear). At the same time there are many scholars on the dynamic characteristics of the diaphragm coupling for more in-depth study, which Hong Chengwen, Zhou Biao deduced and verified the diaphragm coupling axial stiffness of the cyclic changes. The authors study the vibration performance of the helical gear shunt drive system under the parallel unaligned condition of the diaphragm coupling. Firstly, the elastic dynamics model with 14 degrees of freedom of the helical gear shunt system is established, and the corresponding nonlinear vibration differential equation system is built; then, the periodic transverse force generated by the unaligned diaphragm coupling is linked into the vibration differential equation system as the excitation force. Finally, the relationship between the misalignment of the diaphragm shaft coupling and the meshing bias of the system is analyzed according to the results of solving the system of equations.

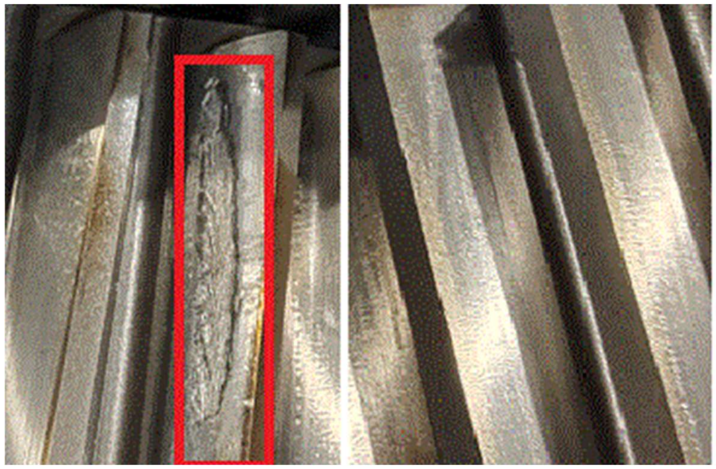

(a) Comparision of meshing wear in second stage

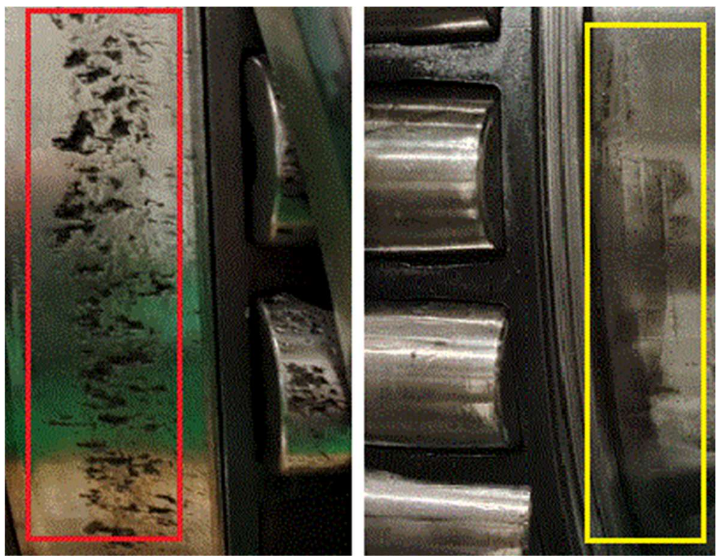

(b) Comparision of bearing wear in second stage

Fig. 1. Comparision of wear in second stage

2. Helical gear shunt drive modeling

2.1. Kinetic modeling

The three-dimensional model of the helical gear shunt drive system is shown in Fig. 2, and the elastic dynamics model of the shunt drive system is constructed using the concentrated mass method, as shown in Fig. 3.

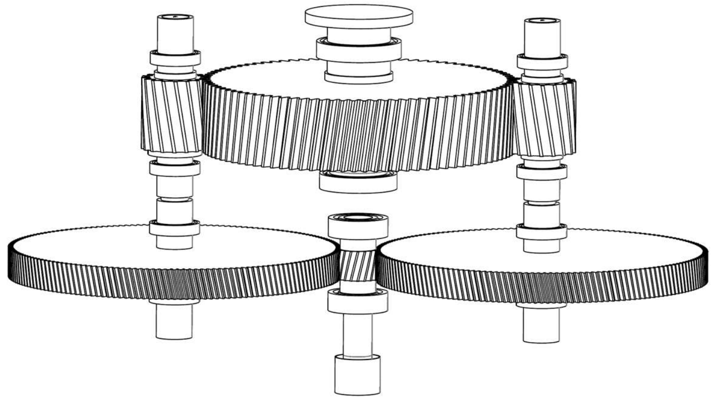

Fig. 2. Power-split transmission system

The centralized mass method was used to construct the elastic dynamics model of the system, as shown in Figure 3. The gear 1,2,3,4,5,6 is defined as $Z_1, Z_2, Z_3, Z_4, Z_5, Z_6$, $m_i\,(i=1,\ 2,\ 3,\ 4,\ 5,\ 6)$, is the mass of gear Z_i, $r_i\,(i=1,\ 2,\ 3,\ 4,\ 5,\ 6)$ is the base circle radius of gear Z_i, $J_i\,(i=1,\ 2,\ 3,\ 4,\ 5,\ 6)$ is the moment of inertia of gear Z_i, $k_{Si}\,(i=1,\ 2,\ 3,\ 4,\ 5,\ 6)$ is the shaft bending stiffness corresponding to gear Z_i, $c_{Si}\,(i=1,\ 2,\ 3,\ 4,\ 5,\ 6)$ is the shaft bending damping coefficient corresponding to gear Z_i, $\theta_i\,(i=1,\ 2,\ 3,\ 4,\ 5,\ 6)$ is the torsional displacement of gear Z_i, $X_i\,(i=1,\ 2,\ 3,\ 4,\ 5,\ 6)$ is the displacement of gear Z_i along the tangent direction of the meshing pair, $k_{Ti}\,(i=0,\ 1,\ 2,\ 3)$ is the torsional stiffness coefficient of input shaft, transmission shaft 1, transmission shaft 2 and output shaft, and $k_{vi1}\,(i=1,\ 2)$ is Z_1 respectively Z_2, Z_3 for the time-varying meshing stiffness, $k_{vi2}\,(i=1,\ 2)$ for Z_6 and Z_4, Z_5 respectively, $C_{vi1}\,(i=1,\ 2)$ for Z_1 with Z_2, Z_3 for the meshing damping coefficient, $C_{vi2}\,(i=1,\ 2)$ for Z_6 and Z_4, Z_5 respectively. J_0, θ_0 are the moment of inertia and torsional displacement of the prime mover; J_7, θ_7 are the moment of inertia and torsional displacement of the load.

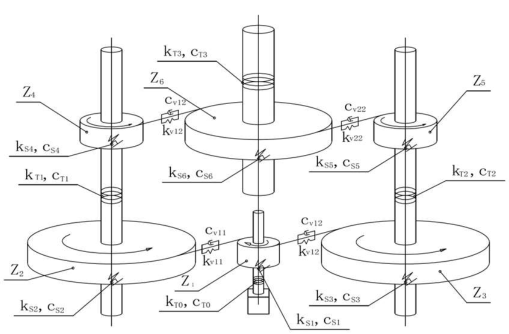

Fig. 3. Model of power-split transmission system

2.2. *Vibrational differential equations of the system*

The bending-torsional vibration differential equations of the system are developed according to the Newton-Euler method:

$$\begin{cases} J_0\ddot{\theta}_0 + c_{T0}\left(\dot{\theta}_0 - \dot{\theta}_1\right) + k_{T0}\left(\theta_0 - \theta_1\right) = T_1 \\ J_1\ddot{\theta}_1 - c_{T0}\left(\dot{\theta}_0 - \dot{\theta}_1\right) - k_{T0}\left(\theta_0 - \theta_1\right) + r_1 F_{11}\cos\beta_1 + r_1 F_{21}\cos\beta_1 = 0 \\ J_2\ddot{\theta}_2 + c_{T1}\left(\dot{\theta}_2 - \dot{\theta}_4\right) + k_{T1}\left(\theta_2 - \theta_4\right) - r_2 F_{11}\cos\beta_1 = 0 \\ J_3\ddot{\theta}_3 + c_{T2}\left(\dot{\theta}_3 - \dot{\theta}_5\right) + k_{T2}\left(\theta_3 - \theta_5\right) - r_3 F_{21}\cos\beta_1 = 0 \\ J_4\ddot{\theta}_4 - c_{T1}\left(\dot{\theta}_2 - \dot{\theta}_4\right) - k_{T1}\left(\theta_2 - \theta_4\right) + r_4 F_{12}\cos\beta_2 = 0 \\ J_5\ddot{\theta}_5 - c_{T2}\left(\dot{\theta}_3 - \dot{\theta}_5\right) - k_{T2}\left(\theta_3 - \theta_5\right) + r_5 F_{22}\cos\beta_2 = 0 \\ J_6\ddot{\theta}_6 + c_{T3}\left(\dot{\theta}_6 - \dot{\theta}_7\right) + k_{T3}\left(\theta_6 - \theta_7\right) - r_6 F_{12}\cos\beta_2 - r_6 F_{22}\cos\beta_2 = 0 \\ J_7\ddot{\theta}_7 - c_{T3}\left(\dot{\theta}_6 - \dot{\theta}_7\right) - k_{T3}\left(\theta_6 - \theta_7\right) = -T_0 \\ m_1\ddot{X}_1 + c_{s1}\dot{X}_1 + k'_{s1}X_1 = F_{11} - F_{21} \\ m_2\ddot{X}_2 + c_{s2}\dot{X}_2 + k'_{s2}X_2 = F_{11} \\ m_3\ddot{X}_3 + c_{s3}\dot{X}_3 + k'_{s3}X_3 = F_{21} \\ m_4\ddot{X}_4 + c_{s4}\dot{X}_4 + k'_{s4}X_4 = F_{12} \\ m_5\ddot{X}_5 + c_{s5}\dot{X}_5 + k'_{s5}X_5 = F_{22} \\ m_6\ddot{X}_6 + c_{s6}\dot{X}_6 + k'_{s6}X_6 = F_{22} - F_{12} \end{cases} \tag{1}$$

In the above equation, F_{11} and F_{21} are the dynamic meshing forces for the upper primary engagement of branch 1 and branch 2, respectively, and F_{12} and F_{22} are the dynamic meshing forces for the upper secondary engagement of branch 1 and branch 2, respectively. k'_{Si} is the equivalent stiffness of k_{Si} when integrated with the corresponding bearing stiffness. Each engagement force can be expressed as:

$$\begin{cases} F_{11} = c_{v11}\dot{Y}_{11} + k_{v11}\cdot f_{11}\left(Y_{11}\right) \\ F_{21} = c_{v21}\dot{Y}_{21} + k_{v21}\cdot f_{21}\left(Y_{21}\right) \\ F_{12} = c_{v12}\dot{Y}_{12} + k_{v12}\cdot f_{12}\left(Y_{12}\right) \\ F_{22} = c_{v22}\dot{Y}_{22} + k_{v22}\cdot f_{22}\left(Y_{22}\right) \end{cases} \tag{2}$$

In the above equation, k_{vij} is the time-varying meshing stiffness of the meshing force F_{ij} corresponding to the meshing pair. Y_{ij} is the engagement force F_{ij} corresponding to the relative displacement of the meshing line of the meshing pair. The torsional displacement of each axle wheel in the system is converted to a line displacement. Y_{ij} can be expressed as:

$$\begin{cases} Y_{11} = \left(-X_1 + r_1\theta_1\right) - \left(r_2\theta_2 + X_2\right) - e_{11} \\ Y_{21} = \left(-X_1 + r_1\theta_1\right) - \left(r_3\theta_3 + X_3\right) - e_{21} \\ Y_{12} = \left(-X_4 + r_4\theta_4\right) - \left(r_6\theta_6 + X_6\right) - e_{12} \\ Y_{22} = \left(-X_5 + r_5\theta_5\right) - \left(r_6\theta_6 + X_6\right) - e_{22} \end{cases} \tag{3}$$

e_{ij} in Equation (3) is the meshing error corresponding to F_{ij}.

$f_{ij}\left(Y_{ij}\right)$ in Equation (2) is the clearance function of the gear mesh pair, and let the mesh clearance be $2b_{ij}$, and b_{ij} is half of the tooth-side clearance of the first i-stage mesh in the first j-branch, then $f_{ij}\left(Y_{ij}\right)$ can be expressed as:

$$f_{ij}\left(Y_{ij}\right)=\begin{cases}Y_{ij}-b_{ij} & Y_{ij}>b_{ij}\\ 0 & -b_{ij}\le Y_{ij}\le b_{ij}\\ Y_{ij}+b_{ij} & Y_{ij}<-b_{ij}\end{cases} \tag{4}$$

In this project, the gear machining accuracy is grade 5, for the first level meshing of the system, b_{11} and b_{12} generate the period segmentation function of time t according to the normal distribution between 0.522 mm~0.851 mm respectively; for the second level meshing of the system, b_{12} and b_{22}, respectively, are generated as period segmentation functions with respect to time t according to a normal distribution between 0.523 mm and 0.853 mm.

3. Equation solving for vibration differential equations

3.1. *Free vibration solution of the system*

Equations (1) (2) (3) (4) are united and solved by applying the 4th order Runge-Kutta method. The dimensionless dynamic dynamic load factor is defined as follows:

$$\begin{cases}G_{11}=\dfrac{F_{11}}{F_{01}}\\ G_{21}=\dfrac{F_{21}}{F_{01}}\\ G_{12}=\dfrac{F_{12}}{F_{02}}\\ G_{22}=\dfrac{F_{22}}{F_{02}}\end{cases} \tag{5}$$

In the above equation, G_{11}, G_{21} are the dynamic load coefficients corresponding to F_{11}, F_{21} respectively, G_{12}, G_{22} are the dynamic load coefficients corresponding to F_{11}, F_{22} corresponding to the dynamic load coefficients, and F_{01}, F_{02} are the theoretical meshing forces of the first and second stage engagement, respectively. Figures 4 and 5 show G_{12} and G_{22}, respectively.

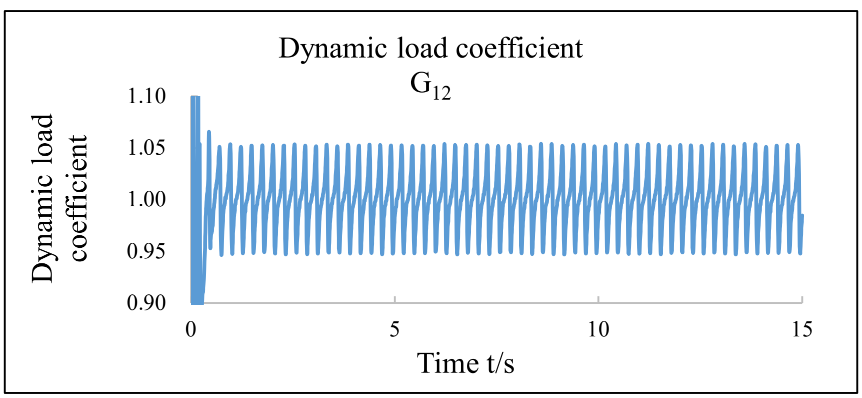

Fig. 4. Dynamic factor G_{12}

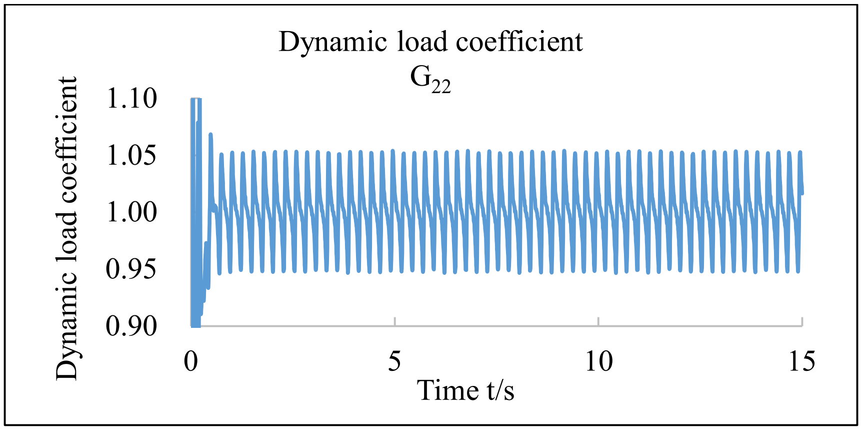

Fig. 5. Dynamic factor G_{22}

It should be noted that although the dynamic load coefficients G_{12} and G_{22} have the same range of fluctuation, there is a phase difference in the period variation of G_{12} and G_{22} due to a phase difference in the time-varying mesh stiffness of the same level of meshing (gear Z_6 has an odd number of teeth).

3.2. *System forced vibration solution*

The lateral stiffness of the diaphragm coupling when not centered has a typical trigonometric form with a period of $T=\frac{2\pi}{N}$, N is the number of connecting bolts on the diaphragm coupling. Coincidentally, the large non-standard diaphragm coupling used for the low-speed shaft that is the subject of this paper happens to be connected by 91 M24 bolts. This number is the same as the number of teeth of Z_6.

The lateral stiffness K_H formula is as follows:

$$K_H=\left(K_{H\max}+K_{H\min}\right)\frac{1}{2}+\left(K_{H\max}-K_{H\min}\right)\cos\left(\frac{n\pi}{60}\right)t \tag{6}$$

In the above equation, $K_{H\max}$ is the maximum transverse stiffness of the coupling, and $K_{H\min}$ is the minimum transverse stiffness of the coupling. The specific value can be obtained by geometric algorithm.

The lateral excitation force generated when the diaphragm coupling is not centered is now solved in Equation (1). Here, the more extreme case is solved first: the phase of the coupling excitation is the same as the corresponding meshing phase of F_{12}, i.e., the excitation is in tune with F_{12}. The results are shown in Figures 6 and 7:

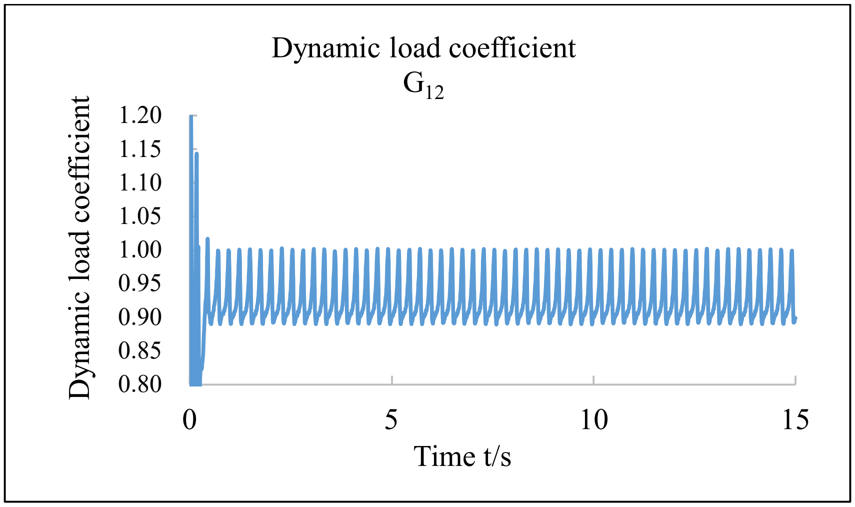

Fig. 6. Dynamic factor G_{12} when exciting force and F_{12} had same phase

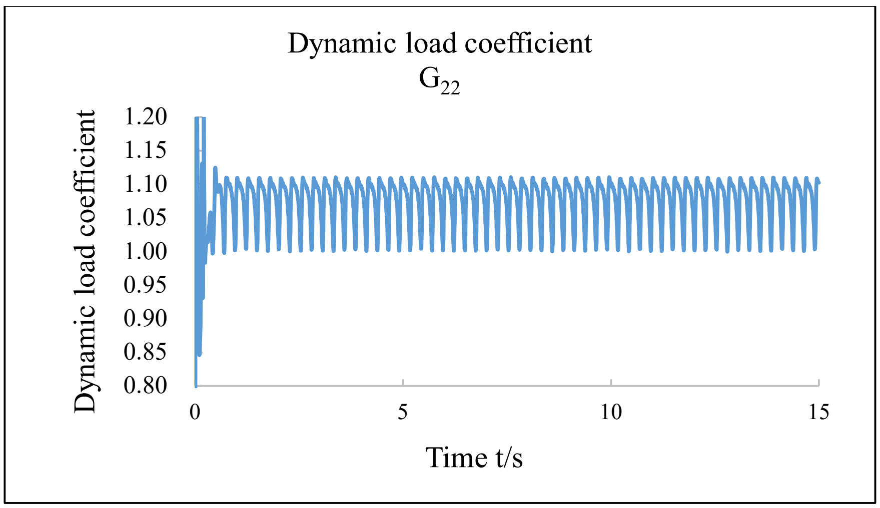

Fig. 7. Dynamic factor G_{22} when exciting force and F_{12} had same phase

It can be seen from Figures 6 and 7 that when the excitation is tapped with one of the secondary meshes, the secondary meshes will be off-loaded, which is the same form of failure as in the actual project (one side of the secondary meshes is frequently damaged with the bearings while the other side is good). This is mainly because the two secondary meshing forces on the gear Z_6 are in opposite directions. However, since it is too costly to replace the gear Z_6 or to change the distribution structure of the coupling bolt set (non-standard diaphragms need to be re-designed), it is now considered that the phase can be changed by changing the relative angle of the bolt holes of the coupling sleeve and the keyway. Let the corresponding meshing phase difference between F_{12} and F_{22} be Φ_1, and the phase difference between the bolt group and F_{12} be Φ_2. Here Φ_1 is a known constant, and different phase difference ratios $W = \frac{\Phi_1}{\Phi_2}$ are solved and averaged to obtain the second stage meshing dynamic loading coefficient-phase difference ratio graph as shown in Fig. 8:

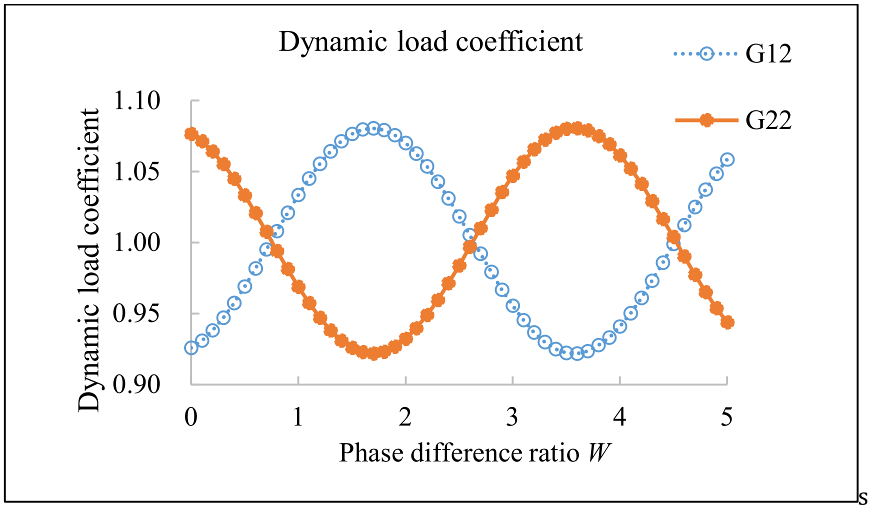

Fig. 8. Relation between Dynamic factor and phase difference ratio W

From Fig. 8, it can be seen that the superposition effect of the excitation force and the meshing force varies with the phase difference ratio, and the mean values of G_{12} and G_{22} will be the same at certain intervals, i.e., the meshing equalizing load performance is optimal. It can be seen that: by adjusting the relative phase of the bolt holes of the coupling sleeve, the meshing equalizing load situation caused by the misalignment of the diaphragm coupling can be effectively improved.

4. Conclusion

1) The 14-degree-of-freedom bending-torsion coupled nonlinear vibration model of helical gear shunt system is established by considering the time-varying meshing stiffness, random tooth side clearance, meshing error, shaft bending deformation and other factors, and the corresponding set of vibration differential equations is established.
2) The time-varying transverse stiffness caused by the misalignment of the diaphragm coupling is introduced into the model and the set of differential equations is set up, and it is found that the phase difference between the bolt group and the mesh has a great influence on the equalizing load condition of the system, and it is verified by comparing with the actual working conditions.
3) The project has been running for more than 18 months after changing the phase of the coupling bolt group through actual modification. During the period after two inspections are found to be abnormal, visible in this paper the theory and practice is consistent.

About the Authors

Zhao Ji was born in Tianjin, P.R. China, in 1989. He obtained a master's degree from JiLin University in China. He is currently working for SEW Industrial GEAR (Tianjin) Co., Ltd. His main research direction is Vibration Characteristics of Gear system.

Meixi Du was born in Tianjin, P.R. China, in 1992. She obtained a master's degree from Beijing forestry University in China. She is currently working for Tianjin Port NO.4 Stevedoring Co., Ltd. Her main research direction is Vibration Characteristics of Gear system.

Xia Li was born in Tianjin, P.R. China, in 1982. She obtained a master's degree from Tianjin University of Science and Technology in China. She is currently working for SEW Industrial GEAR (Tianjin) Co., Ltd. Her main research direction is Vibration Characteristics of Gear system.

References

[1] Lu, Z., Wang, X., Hou, L., Chen, Y., & Li, H. (2018). Dynamic response analysis for the aero-engine dual-rotor-bearing system with flexible coupling misalignment faults. Journal of Vibroengineering, 20(5), 2012-2026.

[2] Guan, Z., Chen, P., Zhang, X., Zhou, X., & Li, K. (2017). Vibration analysis of shaft misalignment and diagnosis method of structure faults for rotating machinery. International Journal of Performability Engineering, 13(4), 337.

[3] Zhang, C., Wang, D., Zhu, R., Chen, W., & Yu, C. (2023). Dynamic modeling and analysis of the rotor-bearing-disc coupling system with misalignment. International Journal of Dynamics and Control, 11(5), 2021-2035.

[4] Desouki, M., Sassi, S., Renno, J., & Gowid, S. A. (2020). Dynamic response of a rotating assembly under the coupled effects of misalignment and imbalance. Shock and Vibration, 2020(1), 8819676.

[5] da Silva Tuckmantel, F. W., & Cavalca, K. L. (2019). Vibration signatures of a rotor-coupling-bearing system under angular misalignment. Mechanism and Machine Theory, 133, 559-583.

[6] Wu, K., Liu, Z., & Ding, Q. (2020). Vibration responses of rotating elastic coupling with dynamic spatial misalignment. Mechanism and Machine Theory, 151, 103916.

[7] Xia, Y., Pang, J., Yang, L., Zhao, Q., & Yang, X. (2019). Study on vibration response and orbits of misaligned rigid rotors connected by hexangular flexible coupling. Applied Acoustics, 155, 286-296.

[8] Tuckmantel, F. W. S., Castro, H. F., & Cavalca, K. L. (2020). Investigation on vibration response for misaligned rotor-bearing-flexible disc coupling system—theory and experiment. Journal of Vibration and Acoustics, 142(2), 021015.

[9] VMS, H., Equbal, A., Equbal, M. I., Khan, Z. A., Badruddin, I. A., & Kamangar, S. (2025). A novel vibration-analysis based reliability quantification model for flexible coupling hub subjected to misalignment. Scientia Iranica.

[10] Ma, P., Li, F., Liu, M., Wang, H., Guo, J., & Han, Q. (2024). Vibrations of a rigid-flexible coupled dual-rotor system under misalignment fault. Journal of Vibration and Control, 10775463251322231.

[11] Liu, Z., Wang, Q., & Guan, H. (2024). Vibration characteristics of a rotating flywheel-flexible coupling system with misalignment fault: Experiment and simulation. Proceedings of the Institution of Mechanical Engineers, Part C: Journal of Mechanical Engineering Science, 238(20), 9840-9855.

[12] Zhang, C., Cao, P., Zhu, R., Chen, W., & Wang, D. (2023). Dynamic modeling and analysis of the spline joint-flexible coupling-rotor system with misalignment. Journal of Sound and Vibration, 554, 117696.

[13] Wang, M., Wen, B., Han, Q., Sun, Y., & Yu, C. (2021). Dynamic characteristics of a misaligned rigid rotor system with flexible supports. Shock and Vibration, 2021(1), 8876190.

[14] Ma, X., Li, Z., Chen, C., & Huang, F. (2024). Nonlinear vibration characteristics of a rotor-bearing system with disc–shaft insufficient interference and flexible coupling misalignment fault. Measurement Science and Technology, 35(12), 125904.

[15] Wang, P., Xu, H., Ma, H., Han, H., & Yang, Y. (2022). Effects of three types of bearing misalignments on dynamic characteristics of planetary gear set-rotor system. Mechanical Systems and Signal Processing, 169, 108736.

[16] Sawalhi, N., Ganeriwala, S., & Tóth, M. (2019). Parallel misalignment modeling and coupling bending stiffness measurement of a rotor-bearing system. Applied Acoustics, 144, 124-141.

[17] Hujare, D. P., & Karnik, M. G. (2018). Vibration responses of parallel misalignment in Al shaft rotor bearing

system with rigid coupling. Materials Today: Proceedings, 5(11), 23863-23871.

[18] Kumar, P., & Tiwari, R. (2021). Dynamic analysis and identification of unbalance and misalignment in a rigid rotor with two offset discs levitated by active magnetic bearings: a novel trial misalignment approach. Propulsion and Power Research, 10(1), 58-82.

[19] Han, Q., Chen, Y., Zhang, H., Jiang, L., & Li, X. (2016). Vibrations of rigid rotor systems with misalignment on squirrel cage supports. Journal of Vibroengineering, 18(7), 4329-4339.

[20] Wang, N., & Jiang, D. (2018). Vibration response characteristics of a dual-rotor with unbalance-misalignment coupling faults: Theoretical analysis and experimental study. Mechanism and Machine Theory, 125, 207-219.

[21] Mehta, G. D., Shelare, S. D., Pachpor, A. A., Sharma, S., Kumar, R., Bisht, Y. S., ... & Abbas, M. (2024). Unravelling the dynamics of misalignment-induced vibrations in two jaw elastomeric couplings for enhanced industrial reliability: a comprehensive analysis of dynamics and diagnostic approaches. Journal of Vibration Engineering & Technologies, 1-14.

[22] Wang, N., Jiang, D., & Yang, Y. (2019). Vibration Modelling and Verification for Rotor-Support-Casing Coupling System with Misalignment Fault. International Journal of Acoustics & Vibration, 24(3).

[23] Xiao, L., Xu, Y., Chen, Z., & Zhang, L. (2023). Non-linear dynamic response of misaligned spline coupling: Theoretical modeling and experimental investigation. Journal of Vibration and Control, 29(7-8), 1590-1605.

[24] Vashisht, R. K., & Peng, Q. (2019). Adaptive hybrid control of unbalanced vibrations of a rotor/active magnetic bearing system with coupling misalignment using low cost instrumentation. Journal of Vibration and Control, 25(15), 2151-2174.

[25] Xu, K., Zhang, Y., & Ming, T. (2021, March). Research on vibration characteristics of propulsion shafting under unbalanced-misaligned coupling fault. In Journal of Physics: Conference Series (Vol. 1802, No. 2, p. 022048). IOP Publishing.